Magnetic Patterning of Permanent-Magnet Rotors for Microscale Motor/Generators

I. Zana*, F. Herrault, D. P. Arnold†, and M. G. Allen
School of Electrical and Computer Engineering, Georgia Institute of Technology, Atlanta, GA 30332, USA
Phone: (404) 894-9419, Fax: (404) 894-5028, Email: mark.allen@ece.gatech.edu
* now with Center for Materials for Information Technology, Univ. of Alabama, Tuscaloosa, AL 35487, USA
† now with Department of Electrical and Computer Engineering, Univ. of Florida, Gainesville, FL 32611, USA

Abstract

We present and characterize a process to pattern magnetic poles on small permanent-magnet (PM) rotors used in microscale, axial-flux, PM machines. Unlike other previously reported approaches, this approach uses a ferromagnetic magnetizing head (MH) and an externally applied magnetic field, and it offers the potential for moderate scalability and batch-magnetization of multiple parts. The process is verified using 8-pole annular PM rotors with thicknesses of 500 μm and 9.5 mm outer diameters. 3-D magnetostatic, finite element analysis (FEA) is employed to examine the process and to verify the experimental magnetization patterns.

Keywords: permanent magnet, magnetic patterning, electric generator, FEMLAB finite element modeling

1. INTRODUCTION

High power-density, microscale, axial-flux, PM machines [1-3] typically employ high-performance magnetic materials, such as SmCo or NdFeB (remanence, B_r=1.0-1.4 T and coercivity, $\mu_0 H_c$=0.8-1.2 T), for the rotor magnet. The alternating axial magnetic poles, required for machine operation, are typically achieved either by using discrete magnets [3] or by impressing a magnetic pole pattern into a mechanically contiguous magnet [1, 2]. For the latter approach, magnetic patterning is achieved by applying high-intensity magnetic fields to selected regions of a magnet to define the magnetization pattern. These spatially confined magnetic fields can be achieved by passing currents through conductors of an appropriate shape [4, 5] or by concentrating magnetic fields in specific regions using shaped, high-permeability, ferromagnetic, magnetizing heads (MHs) [6].

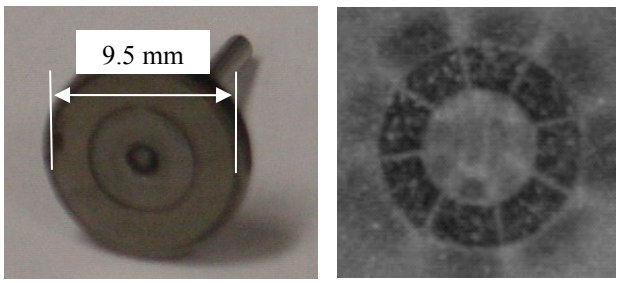

Figure 1. (a) 8-pole SmCo rotor (Thickness = 0.5 mm, OD=9.5 mm) encased in a Ti adaptor used for microscale power generator [1]; (b) qualitative view of the magnetic pattern as evidenced by magnetic paper.

Most recent investigations for microscale PM power generators use thin (< 1 mm), disc or annular rotor magnets with relatively large outer diameters (OD=8-10 mm) [1,2,6]. One such rotor for a recently reported machine is shown in Fig.1 [1]. Design optimization for this particular device indicates that an 8-pole rotor yields the optimal output power [7]. However, to further reduce the size of these types of devices and enable true batch-fabrication requires a magnetizing process able to achieve both small pole-pitch and simultaneously magnetize multiple rotors in parallel. Therefore, in the present paper, we present a process that addresses both these requirements.

2. MAGNETIC PATTERNING PROCESS

In the proposed process, a PM rotor is sandwiched between two conventionally machined FeCoV MHs, as shown in Fig.2. Under an externally applied magnetic field, the high-permeability MHs act to concentrate the fields in the gap between the teeth, while partially shielding the areas not between the teeth (termed slots). Due to the high saturation of FeCoV (B_s=2.4 T), a high magnetic field is produced in the gap between the teeth when the two heads are in close proximity to each other (less than the pole width).

This process is similar to that reported in [6], but utilizes an externally applied pulsed magnetic field from a pulse-discharge magnetizer, rather than an integrated coil winding. This approach offers three advantages. First, eliminating the integrated winding permits simpler MH design and fabrication. Second, it offers the potential for better scaling—smaller rotors may be magnetized without the possibility of exceeding the maximum current density of suitably scaled windings. Third, it enables the possibility of magnetization of numerous rotors in parallel using multiple

magnetizing heads and only one external coil (from the magnetizer).

In practice, a SmCo rotor is first uniformly magnetized (without the MHs) using a pulse-discharge magnetizer (Oersted Technology). Then, using the MHs, selected regions are reversed. Specifically, the magnetic regions in the gap between the teeth of the MHs are reversed, while the slots regions are not. The magnitude of the fields generated in the gap between the MHs teeth must be large enough to reverse the magnetization, but not too large where stray leakage flux reverses the slots regions, thus the entire magnet. Therefore, the externally applied magnetic field must be tailored in order to achieve the desired pole pattern.

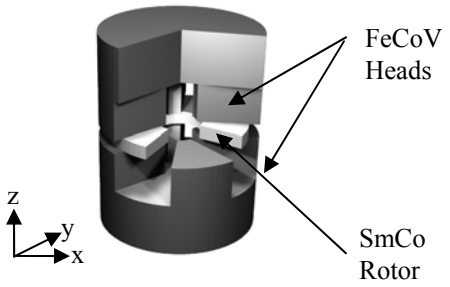

Figure 2. Cutaway view of the magnetizing fixture used for patterning poles on permanent magnet rotors.

3. MODELING AND VALIDATION

In order to examine the magnetization process and to verify the experimental magnetization patterns, several 3D finite-element models were developed using FEMLAB 3.1.

3.1 Examination of the magnetization process

The magnetizing process is carried out using a pulse-discharge magnetizer, inherently a time-varying process. However, due to the limitation in computing resources, a 3D nonlinear magnetostatic finite element model (FEM) was used to examine the magnetic fields in the gap between the magnetizing heads (without the presence of the PM rotor, which was modeled as air). This model does not take into account time-dependent effects (*i.e.* eddy currents), but is used to simulate the field distribution at the peak of the pulsed field.

Due to symmetry, only a quarter of the magnetizing assembly was modeled. The magnetizing heads were assigned a nonlinear, experimentally determined relative magnetic permeability (μ_r, as measured by a vibrating sample magnetometer), while the surrounding air elements and the PM were assigned $\mu_r = 1$. Everywhere, magnetic insulating boundary conditions ($n \cdot B=0$) except at the top and bottom, where an inward flux density ($-n \cdot B=B_n$) and zero potential ($V_m=0$), were imposed, respectively. This simulates the magnetizing head in an uniform magnetic flux density. The finite-element package uses a stationary nonlinear solver to determine the magnetic scalar potential (V_m), from which the magnetic field is computed.
Maps of the z-component of the magnetic flux density (B_z), at the midpoint between the magnetizing heads, as well as cross-sections in the x-y and y-z planes were taken as output for further analysis. In Fig.3(a) and (b) two such plots are shown which demonstrates the beneficial effect of the CoFeV MH concentrating the magnetic flux between the teeth.

To verify the magnetization process, field measurements were made on adjacent poles of a magnetized PM rotor. The maximum measured up and down fields were termed B(+) and B(-), respectively, and their sum and difference termed as ΣB and ΔB, respectively. The measurements were obtained using a Hall sensor (0.2 mm x 0.2 mm active area) 250 μm above the magnet surface. Optimum magnetization was deemed when the measured fields were equal and opposite (ΔB maximized and $\Sigma B \approx 0$).

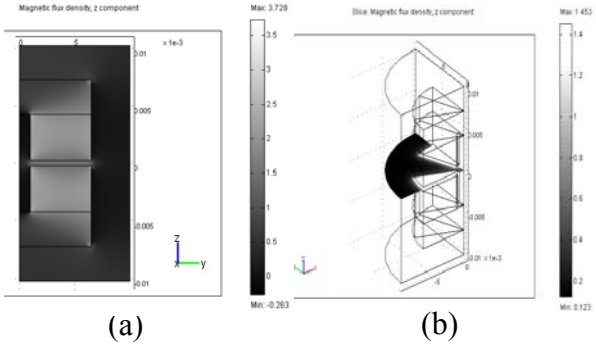

Figure 3. (a) Cross-section of the 3D model, showing the distribution of the z-component of the magnetic flux density, B_z; (b) Concentrating magnetic flux as evidenced by the slice plot of the B_z at midpoint between the MH.

Fig.4(a) and (b) show the difference (ΔB) and sum (ΣB), as a function of energy applied by the pulse-magnetizer. It was noticed experimentally (Fig.4(a)) that a specific energy, set by the capacitance and initial voltage of the pulse-discharge magnetizer, was necessary to achieve high magnetic fields as well as good balance between the up and down poles of a magnetized rotor. If a large pulse was applied, the entire magnet would be reversed, likely due to leakage flux. Conversely, a very small pulse would not overcome the magnetic anisotropy of the already magnetized structure, and thus would not reverse the magnetization. For this particular case, at a specific energy (~3.8 kJ), a maximum amplitude was achieved, as well as a good balance.

Insight into this process was gained by simulating the magnetizing fields between the MHs under progressively larger applied magnetic flux densities (B_{ext}). A qualitative understanding of the experimental data is provided by the

calculated magnetic flux densities at the midpoints between the MH teeth and MH slots, as depicted in Fig. 4(c). For very low B_{ext} (below 0.2 T), the resulting magnetic flux density between the teeth is insufficient to overcome the anisotropy of the magnet ($\mu_0 H_k \sim 2$ T). As B_{ext} increases, the magnetic flux density between the teeth increases and will begin to reverse and ultimately fully reverse the magnetization. However, the magnetic flux density in between the slots is also increasing, and above some threshold, the magnetic regions between the slots will also start to reverse. For example, a B_{ext}=1.5 T produces a reversal magnetic flux density of 1 T in between the slots, presumably sufficient to partially reverse that region.

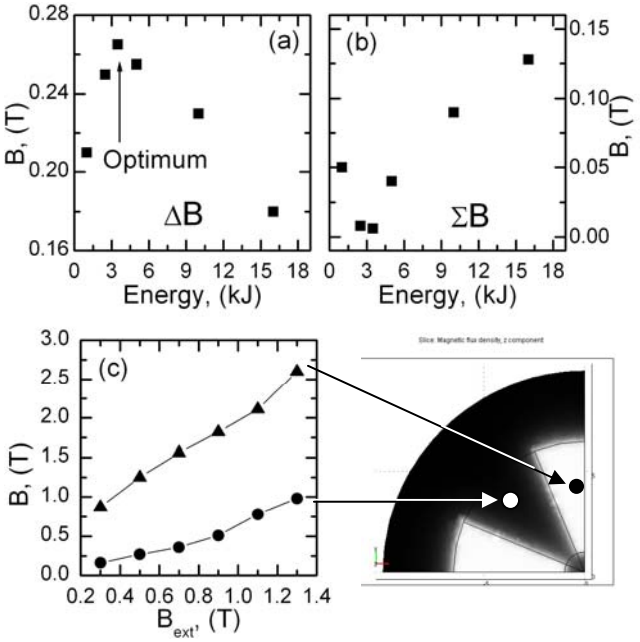

Figure 4. Experimental results: (a) ΔB indicates the amplitude difference between two adjacent poles; (b) ΣB indicates how well "balanced" the magnetization is. FEM model results: (c) calculated B_z at midpoint between MHs.

3.2 Verification of the pole pattern of a SmCo rotor

A 3D linear magnetostatic FEM was used to model the fields from an 8-pole magnetized rotor for comparison with experimental measurements. Again, due to the symmetry, only a quarter (two adjacent half poles) of the PM rotor was modeled. The two half poles were assumed uniformly magnetized with a B_r = 1 T and μ_r = 1 (typical for SmCo), and a sharp transition at their boundary. Outside, magnetic insulation boundary conditions were used to account for the symmetry.

Experimentally, B_z was mapped across the entire surface of a SmCo rotor (OD=9.5 mm, ID=5.0 mm thickness=0.5 mm) at a height of 250 µm above the rotor, as shown in Fig.5(a). An x-y positioning stage was used to scan a Hall probe in 500 µm step increments, by means of two stepper motors controlled by a Matlab application. The experimental B_z map was then compared to the data predicted by FEM. Fig.5(b) shows a slice plot of the predicted B_z, at 250 µm above the surface for comparison to the experimental measurements in Fig.5(a). Good agreement in both profile and amplitude is observed, thus verifying proper magnetization of the PM rotor.

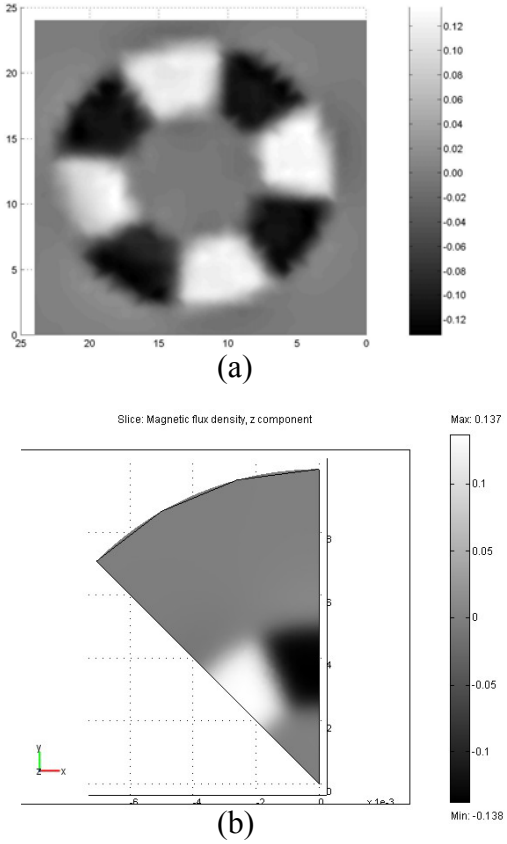

Figure 5. Experimental B_z map acquired at 250 µm above the rotor (a), showing good agreement with the calculated field map (b).

4. PROCESS SCALABILITY

Scaling down the magnetizing process to smaller diameter rotors is enabled by circumventing the requirement to fit the windings into the MH body, as compared to a previous process [6]. Based on the good correlation between experimental and calculated data, a 3D model of the MHs has been constructed with the intent of investigating the potential of using the same process to magnetize 8-pole rotors of the same thickness but having smaller radial dimensions. An external magnetic field of B_{ext}=1.1 T was imposed because it provides sufficient reversal flux density between the teeth, while minimizing the leakage flux between the slots. As before, a nonlinear μ_r was used for the soft magnetic material.

The distribution of B_z on an x-y plane located at the midpoint between the MHs is shown in Fig.6(a). Also, the radial distribution of B_z along the lines indicated in Fig.6(a), are shown in Fig.6(b). In order to properly magnetize a rotor, the difference in the B_z between two points on the same radius, should be as large as possible. Also, the B_z in the slot region must be small to avoid inadvertent reversal. As seen, a SmCo rotor with an inner radius (R_i) < 1.5 mm would be subjected to a significant (> 0.9 T) stray reversal magnetic flux density in the slot region. This may lead to an unbalanced pattern, or even a total reversal. This type of analysis may be used to determine the minimum rotor dimensions suitable for this type of magnetization.

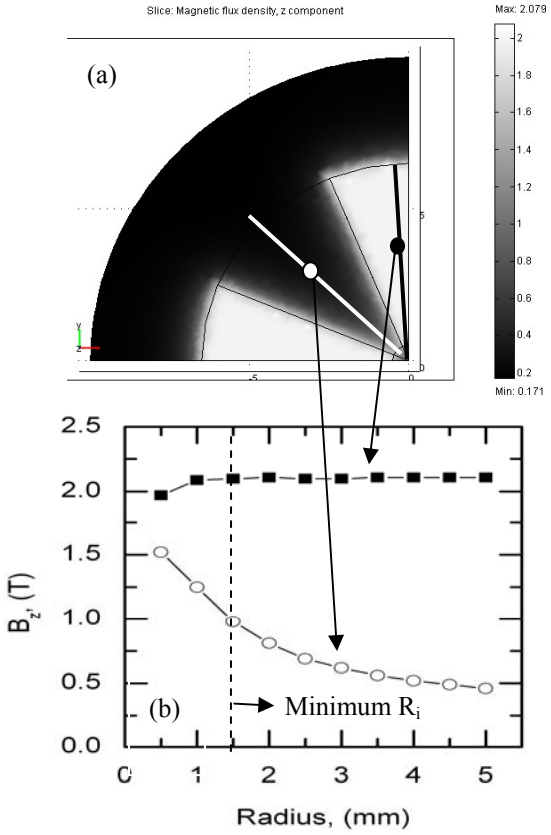

Figure 6. (a) Slice plot of B_z at midpoint between the MHs, for an external field of 1.1 T; (b) calculated radial distribution of B_z along the lines indicated in (a).

5. CONCLUSIONS

A process for patterning magnetic poles on small permanent-magnet (PM) rotors used in microscale, axial-flux, PM machines has been presented. The process presented facilitates the patterning of rotors of various diameters using a pair of ferromagnetic MHs. However, this process may be extended to support batch magnetization of multiple rotors using multiple pairs of MHs, their number being limited primarily by the size of the magnetizer coil.

The process has been examined both experimentally and theoretically. Qualitative understanding of the magnetization process was gained using 3D finite-element models. The models correlate well with experimentally observed phenomena. Most convincingly, the measured fields for an 8-pole SmCo rotor match the predicted fields, indicating the magnetization process works successfully.

Due to its ability to account for stray (leakage) magnetic fields, additional finite-element modeling was employed to investigate the scalability of this process for smaller rotors. It was theoretically shown that annular, 8-pole rotors could be patterned down to an inner radius of 1.5 mm (assuming a rotor thickness of 0.5 mm).

Similar models could be used to determine the suitability of this approach for a wide variety of magnet sizes, shapes, and or pole patterns, as well as to predict the performance of batch patterning using multiple MHs.

ACKNOWLEDGMENTS

This work was supported by the United States Army Research Laboratory Collaborative Technology Alliance (DAAD19-01-2-0010).

REFERENCES

[1] S. Das, *et al*.., "Multi-watt electric power from a microfabricated permanent-magnet generator," *MEMS 2004*, pp. 287-290.
[2] H. Raisigel, et al., "Magnetic planar micro generator," MEMS 2005, pp. 757-761.
[3] A.S. Holmes, G.Hong, and K.R. Pullen, "Axial – flux permanent magnet machines for micropower generation", J. Micromechanical Sys., vol.14, pp.54-62, 2005.
[4] J. Topfer and V. Christoph, "Multi-pole magnetization of NdFeB sintered magnets and thick films for magnetic micro-actuators," *Sens. & Act. A*, v.113, p. 257, 2004.
[5] C. D. Riley, G. W. Jewell, and D. Howe, "The design and analysis of axial field multipole impulse magnetizing fixtures," *J. App. Physics*, v.83, p.7112, 1998.
[6] P.-A. Gilles, J. Delamare, and C. Cugat, "Rotor for a brushless micromotor," *J. Magn. & Magn. Mat.*, 2002.
[7] D. P. Arnold, *et.al.* , "Optimization of a microscale, axial-flux, permanent–magnet generator", PowerMEMS 2005, concurrent submission.